Some Dynamical Aspects of Precipitating Convection

KERRY A. EMANUEL

Center for Meteorology and Physical Oceanography, Massachusetts Institute of Technology, Cambridge, MA 02139

(Manuscript received 16 December 1985, in final form 14 April 1986)

ABSTRACT

A simple linear model is developed with the idea of demonstrating the basic physical processes that serve to distinguish the dynamics of precipitating convection from those of the nonprecipitating variety. In particular, it is shown that the hypothesis advanced by Seitter and Kuo to explain the slope and propagation of squall lines in the context of a fully nonlinear numerical model operates also within a linear model. With a hierarchy of linear models, it is demonstrated that 1) precipitating convection in a basic state consisting of a resting, uniform, unstable cloud can propagate and exhibit sloping up- and down-drafts; 2) subcloud evaporation of falling precipitation leads to modifications of the aforementioned instabilities and the formation of a new mode that travels rapidly and has peak amplitude in the subcloud layer; and 3) the introduction of a shear layer at the cloud base serves to couple the subcloud layer mode mentioned here with the cloud layer and yields a deep, rapidly growing, down-shear propagating mode which, while it has no critical level, nevertheless extracts kinetic energy from the mean shear. These models predict that small vertical shear favors slow-moving shear-parallel squall lines, somewhat larger shear leads to fast-moving shear-perpendicular lines, and very large shear favors three-dimensional convection.

1. Introduction

Among the many aspects of moist convection that continue to elude scientific explanation is the tendency of some convective systems to organize themselves in lines or arcs, sometimes far away from preexisting quasi-linear structures such as fronts. These lines often propagate with respect to the background flow at all levels (Zipser, 1977) and may be aligned parallel to the mean vertical shear (Newton, 1950), perpendicular to it (Barnes and Sieckman, 1984), or at odd angles to it (Bluestein and Jain, 1985). Virtually all theories of nonprecipitating convection show a strong tendency for the convection to occur in lines oriented parallel to the vertical shear. These studies include analytic solutions and integral relations from linear theory (Kuo, 1963), numerical simulations (Deardorff, 1965; Asai 1970a,b), and analytic nonlinear steady-state models (Moncrieff and Miller, 1976; Moncrieff, 1981).[1] At the same time, models of moist convection which allow for stable, unsaturated downdrafts (e.g., Lilly, 1960; Bretherton, 1986) show a clear preference for three-dimensional clouds, at least in unsheared environments. Thus both the orientation and the quasi-two-dimensionality of many squall lines remain unexplained by simple theories.

The propagation of convective systems has also been the subject of much controversy. Of particular interest is the propagation of some tropical squall lines with respect to the background wind at all levels (e.g., Zipser, 1977), and the movement of supercell thunderstorms at velocities which systematically depart from the background hodograph (Browning and Ludlam, 1962). In the latter case, an attractive and apparently correct explanation for the deviant propagation in terms of pressure perturbations arising from the storm–mean flow interaction has been advanced by Rotunno and Klemp (1982). This explanation has been rather thoroughly tested against numerical simulations of supercell thunderstorms. The great longitudinal extent of squall lines, however, has restricted their simulation by three-dimensional numerical models; such simulations have only recently been attempted (M. Weisman, personal communication, 1986). Among the more popular simple theories of squall line formation and propagation is the "Wave-CISK" (Conditional Instability of the Second Kind) theory advanced by Lindzen (1974) and advocated by many others, including Raymond (1975, 1976, 1983, 1984), Bolton (1984), and Emanuel (1982). This theory holds that mesoscale convective systems are manifestations of a constructive interaction between cumulus convection and internal inertia–gravity waves, the latter of which strongly govern the propagation velocity of the systems. Such a constructive interaction has never been determined from observations, however; nor have numerical simulations which explicitly resolve cumulus convection shown wave-CISK behavior. A recent attempt by Nehrkorn (1986)

[1] An exception occurs in the work of Kuo and Seitter (1985) who found intermediate modes for cases of complex wind fields for which the direction of the shear changes strongly with height. For these wind profiles it is not clear what shear to define parallel and perpendicular with respect to.

to account for both the propagation and orientation of squall lines with respect to the background vertical shear using wave–CISK theory showed that while model parameters could be adjusted to obtain the observed orientation, phase speeds were then too large by a factor of from 2 to 5.

An attractive alternative to the wave–CISK view of squall lines has recently been advanced by Seitter and Kuo (1983). They pointed out that in nonprecipitating convection, buoyancy is a function of vertical displacement alone. This strong dynamical constraint prevents any propagating behavior (Bolton, 1980) and also prevents the divergent component of the convective circulation from extracting kinetic energy from constant background shear (Emanuel, 1984). In precipitating convection, however, important sinks of buoyancy due to condensate loading, evaporation and melting of falling water are gravitationally uncoupled from vertical displacement of air parcels. By means of fully nonlinear, two-dimensional numerical simulation Seitter and Kuo (1983) were able to show that this dephasing of buoyancy generation from updrafts can lead to propagation and extraction of kinetic energy from background shear. This is an important finding as it potentially explains the orientation, phase speed and slope of observed squall lines. The purpose of the present paper is to show that the basic dynamics of the mechanisms discussed by Seitter and Kuo (1983) can be described in the context of simple linear models of precipitating convection. While such models leave out many important physical processes, they have the advantage of clearly illuminating the operation of the particular dynamical mechanisms which are incorporated by design. Moreover, certain predictions of the models can be at least qualitatively compared with nature as a means of assessing the relative importance of the processes included in the model.

We proceed in section 2 to derive a set of inviscid equations linearized about a basic state which contains a uniform suspension of very small cloud droplets. A linearization of Kessler's (1969) microphysical representations describes the evolution of the rainwater field. This "bare bones" linear model describes the elementary effects of rainwater loading on convective dynamics; it is shown that these effects lead to sloping updrafts and slow propagation provided the rainwater loading is not small compared to the thermal buoyancy. Elementary effects of subcloud evaporation of rain are described in section 3 by adding a neutrally stratified dry subcloud layer to the basic state discussed in section 2. The presence of the subcloud layer leads to modifications of the modes described in section 2 and introduces new modes as well. When a discontinuous velocity profile is added to this basic state (section 4), the new modes are preferentially amplified and for a range of shear values the growth rates exceed those in the no-shear case. It is shown that these modes extract kinetic energy from the mean shear but do not have a critical level. We summarize these results in section 5 and construct a tentative regime diagram showing the optimum forms of precipitating convection as a function of mean shear and stability.

2. Effects of precipitation drag

We first consider a basic state consisting of a uniform suspension of water droplets in resting air contained between two infinite parallel plates the upper of which is maintained at a smaller temperature than the lower. The mixture of air and water droplets is in thermodynamic equilibrium so that the air is just saturated everywhere, and the system is in hydrostatic balance. We consider the stability of this system to small perturbations whose time scale is large compared to the time scale of condensation, so that the system is always in thermodynamic equilibrium. For maximum simplicity we consider two-dimensional perturbations which are inviscid and Boussinesq. The linearized equations for vorticity in the x–z plane and thermal buoyancy are

$$\frac{\partial}{\partial t}\nabla^2\psi = \frac{\partial B}{\partial x} - g\frac{\partial l}{\partial x}, \tag{1}$$

$$\frac{\partial B}{\partial t} = N^2\frac{\partial \psi}{\partial x}, \tag{2}$$

where ψ is the streamfunction, defined so that

$$w = \frac{\partial \psi}{\partial x}, \quad u = -\frac{\partial \psi}{\partial z},$$

B is the perturbation thermal buoyancy ($g\theta'_v/\theta_{v0}$, where θ'_v and θ_{v0} are perturbation and reference virtual potential temperatures), l is the perturbation liquid water content per unit mass, and N^2 is a measure of the unstable stratification:

$$N^2 \equiv -g\frac{\Gamma_m}{\Gamma_d}\frac{\partial \ln\bar{\theta}_e}{\partial z},$$

where Γ_m and Γ_d are the moist and dry adiabatic lapse rates, g is the acceleration of gravity and $\bar{\theta}_e$ is the mean state equivalent potential temperature (Durran and Klemp, 1982). In eqs. (1) and (2) B may be interpreted as the buoyancy due to all effects except condensate loading.

Note that the second term on the right side of (1) represents the generation of vorticity by perturbation liquid water drag. In order to close the system of linear equations, a predictive equation for perturbation liquid water must be developed. For this purpose, we linearize a system of equations representing cloud microphysics developed by Kessler (1969), who divided the total condensate field into cloud water (l_c), which is advected with the flow, and rainwater (l_R), which may fall at a terminal velocity V_T (here taken to be positive). Kessler's rate equations for l_c and l_R, specialized to a sat-

urated Boussinesq fluid and neglecting collisions between rainwater and cloud water, may be written

$$\frac{dl_c}{dt} = -\frac{\partial \psi}{\partial x}\frac{dq_s}{dz} - k(l_c - a), \tag{3}$$

$$\frac{dl_R}{dt} = V_T\frac{\partial l_R}{\partial z} + k(l_c - a), \tag{4}$$

where q_s is the saturation mixing ratio, V_T is here considered constant, a is the "autoconversion threshold" cloud water content, and k is defined

$$k \equiv \begin{cases} k_1 & \text{if} \quad l_c > a \\ 0 & \text{if} \quad l_c \leqslant a. \end{cases} \tag{5}$$

The rate equations include growth of cloud droplets by condensation, changes of rainwater content by gravitational fallout, and conversion from cloud water to rainwater at a rate which depends on the amount of cloud water exceeding the autoconversion threshold a. We consider the base state cloud water in our linear model to exactly equal the autoconversion threshold amount a, so that the (almost) linear counterparts of (3)–(5) are

$$\frac{\partial l_c'}{\partial t} = -\frac{\partial \psi}{\partial x}\frac{dq_s}{dz} - kl_c' \tag{6}$$

$$\frac{\partial l_R}{\partial t} = V_T\frac{\partial l_R}{\partial z} + kl_c', \tag{7}$$

$$k \equiv \begin{cases} k_1 & \text{if} \quad l_c' > 0 \\ 0 & \text{if} \quad l_c' \leqslant 0, \end{cases} \tag{8}$$

where primes denote departures from base state values. The conditional nature of the conversion from cloud water to rainwater, reflected by (8), imposes an essential nonlinearity in the system analogous to the mathematical problem of moist convection treated by Lilly (1960), Bretherton (1986) and others. In the interest of maintaining the maximum simplicity, we must simplify the condition (8) while recognizing that certain fundamental aspects of the problem will be missed. We will later argue that the effects illuminated by the strictly linear model should have qualitative counterparts in more complete treatments of the problem. For the present, then, we shall simply take k to be a constant irrespective of the sign of l_c. Physically, this means that contours of cloud water deficit as well as rainwater fall at velocity V_T.

The addition of (6) and (7) results in a relation for the total perturbation water content, l:

$$\frac{\partial l}{\partial t} = V_T\frac{\partial l_R}{\partial z} - \frac{\partial \psi}{\partial x}\frac{dq_s}{dz},$$

where $l = l_c' + l_R$. Taking the limit of large k in (6) and (7) we find that $l_c' \to 0$ and $l_R \to l$ so that the above becomes

$$\frac{\partial l}{\partial t} - V_T\frac{\partial l}{\partial z} = -\frac{\partial \psi}{\partial x}\frac{dq_s}{dz}. \tag{9}$$

The system comprised of (1), (2) and (9) may be regarded as the maximally simple system which includes the effects of condensate loading and fallout. We also consider a system for which the temperature difference between the plates is small enough so that dq_s/dz and N^2 may be regarded as constants. The set of equations we will solve is summarized:

$$\frac{\partial}{\partial t}\nabla^2\psi = \frac{\partial B}{\partial x} - g\frac{\partial l}{\partial x}, \tag{10}$$

$$\frac{\partial B}{\partial t} = N^2\frac{\partial \psi}{\partial x}, \tag{11}$$

$$\frac{\partial l}{\partial t} - V_T\frac{\partial l}{\partial z} = -\frac{\partial \psi}{\partial x}\frac{dq_s}{dz}, \tag{12}$$

where N^2, V_T and dq_s/dz are constants.

a. *Normal modes in an infinite domain*

Wavelike solutions to the set (10)–(12) can be found by considering normal modes in an unbounded domain. Noting the existence of internal length and time scales, we first nondimensionalize the dependent and independent variables as follows:

$$x^*, z^* = V_T N^{-1}(x, z),$$
$$t^* = N^{-1}t$$
$$B^* = V_T N B,$$
$$\psi^* = V_T N^{-1}\psi,$$
$$l^* = -\frac{dq_s}{dz}V_T N^{-1} l,$$

where the asterisks denote the dimensional values. The length scale $V_T N^{-1}$ is the only internal scale present and represents the distance rain falls in the convective time scale N^{-1}. As will be shown later, this internal scale, together with an externally imposed vertical scale, partially determines the slope of the convection.

Assuming normal mode solutions of the form $e^{\sigma t + i(rz + kx)}$, where σ is the (complex) growth rate, and r and k are (real) vertical and horizontal wavenumbers, the following cubic dispersion relation for σ results:

$$\sigma^2 = \beta\left[1 - \frac{\alpha\sigma}{\sigma - ir}\right], \tag{13}$$

where $\beta \equiv (1 + r^2/k^2)^{-1}$ and α is the sole dimensionless parameter in the system:

$$\alpha \equiv -g\frac{dq_s}{dz}N^{-2}. \tag{14}$$

This parameter may be interpreted as the ratio of condensate drag to all other sources of buoyancy generated by a reversible displacement, and is related to the quantity MCAPE defined by Seitter and Kuo (1983) by

$$\text{MCAPE} = \tfrac{1}{2}N^2H^2(1 - \alpha),$$

where H is the vertical scale through which MCAPE is defined. In (13) β is clearly related to the slope of the disturbances but the vertical wavenumber (r) enters separately as well. In the special case $\alpha = 0$, the solution to (13) ($\sigma^2 = \beta$) represents the solution of the classical inviscid convection problem for which the growth rate is maximized when the disturbances are vertical ($\beta = 1$).

General solutions may be found by solving the cubic equation (13) exactly. The growth rate σ_r and phase speed ($c = -\sigma_i/k$) of the disturbances are shown in Figs. 1 and 2 for the cases $r = 0.2$ and $r = 0.8$. The sign of c is always opposite the sign of the slope of the disturbances in the x–z plane. At large values of α and small values of r, the growth rate reaches a maximum at values of β between 0 and 1 indicating a preference for modes with a finite slope in the x–z plane. Phase speeds of the modes (Fig. 2) increase with α; recall that they are scaled by the fall speed V_T. Naturally, there is no preference for direction of propagation in this system, nor are two-dimensional modes preferred over three-dimensional convection.

The solutions for growth rate shown in Fig. 1 imply that for a given value of r there exists a critical value

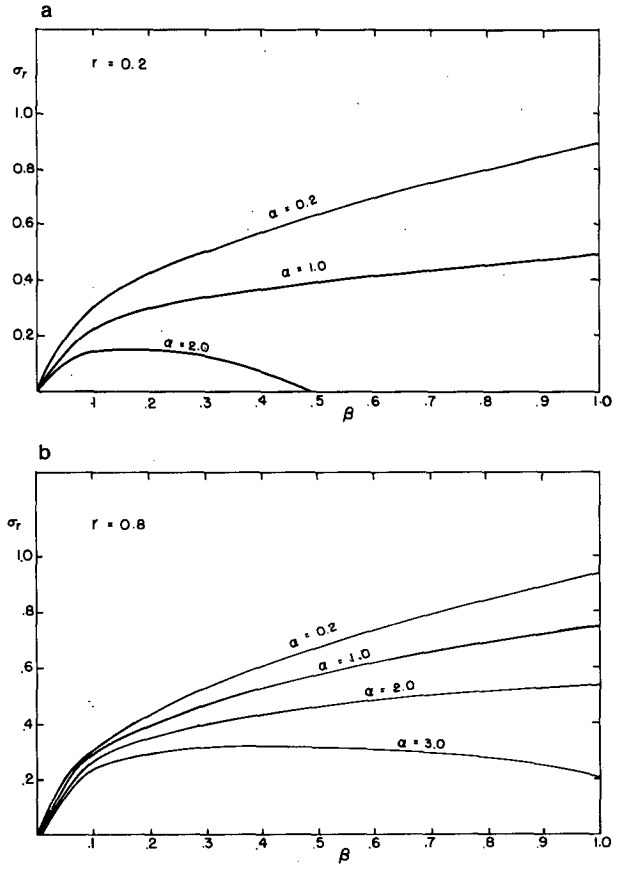

FIG. 1. Dimensionless growth rates of unbounded modes as a function of β for several values of α. Vertical wavenumber (a) $r = 0.2$ and (b) $r = 0.8$.

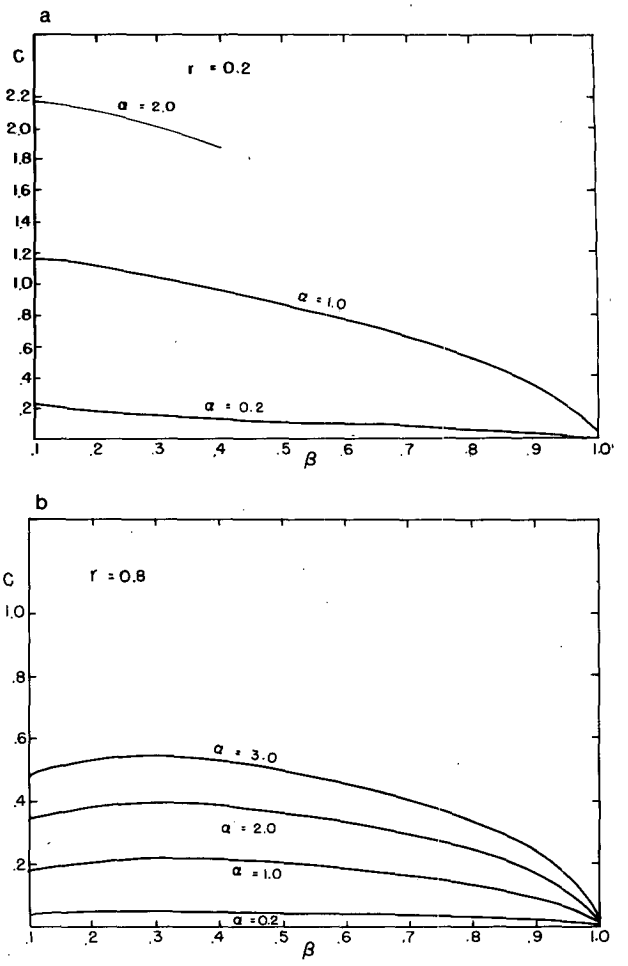

FIG. 2. As in Fig. 1 but showing dimensionless phase speeds.

of α above which growing disturbances cannot exist. This critical value can be found by taking the limit of (13) as the real part of $\sigma(\sigma_r)$ goes to zero. We find that the critical value of α satisfies the relation

$$1-(1+3\chi(\alpha-1)^{1/2} = 3\chi(\alpha-1)\left[\left(1-\frac{3}{\chi(\alpha-1)^2}\right)^{1/2}-1\right], \quad (15)$$

where $\chi \equiv \beta/r^2$. The solution to the above corresponds to a disturbance frequency given by

$$\sigma_i = \frac{r}{3}\{1-[1+3\chi(\alpha-1)]^{1/2}\}. \quad (16)$$

In the limit of small χ, the solutions are

$$\lim_{\chi\to 0}\alpha_c = 1+2r/\sqrt{\beta},$$
$$\lim_{\chi\to 0}\sigma_i = -\sqrt{\beta}. \quad (17)$$

Thus, for β small and/or r large the critical value of α can be quite large, though inspection of Fig. 1 shows

that growth rates associated with large α will be small. The existence of growing solutions for α greater than one shows that precipitating convection can be maintained even when MCAPE, as defined by Seitter and Kuo (1983), is negative; though as the latter point out, convection cannot be initiated in such an environment due to the finite time needed to form precipitation. In the present model, condensate begins to fall immediately upon forming so that growing solutions may conceivably exist as long as the thermal buoyancy (N^2 or α) is positive.

The propagation and slope of the disturbances is related to the gravitational de-phasing of condensate loading from the updraft. The reader is referred to Seitter and Kuo (1983) for a concise explanation of the physical mechanism. The possibility of oscillatory convection associated with falling precipitation was perhaps first considered by Kessler (1969).

b. *Solutions between parallel plates*

Somewhat more interesting solutions can be obtained by considering the basic state to be bounded above and below by rigid horizontal plates separated by a distance H. This introduces an external length scale into the system and it is convenient to renormalize the dependent and independent variables which appear in (10)–(12). The new dimensionless variables are defined as follows:

$$\begin{aligned} x^*, z^* &= H(x, z), \\ t^* &= N^{-1}t, \\ B^* &= N^2HB, \\ \psi^* &= H^2N\psi, \\ l^* &= -(dq_s/dz)Hl, \\ V_T^* &= NHV_T, \end{aligned} \tag{18}$$

where the asterisks again denote the dimensional variables. We now substitute normal mode solutions of the form

$$F(z)\exp(\sigma t + ikx)$$

and eliminate β and l in favor of ψ. The resulting third-order ordinary differential equation for the vertical structure of ψ is

$$\sigma^2 V_T \frac{d^3\psi}{dz^3} - \sigma^3 \frac{d^2\psi}{dz^2} + V_T k^2(1-\sigma^2)\frac{d\psi}{dz} + \sigma k^2(\sigma^2 + \alpha - 1)\psi = 0. \tag{19}$$

Besides the conditions forbidding flow normal to the two boundaries, a third boundary condition is required. For this we take l to vanish along the upper boundary so that no condensate may fall into the system from above. A consequence of this condition that follows from (10) and (11) is that $d^2\psi/dz^2$ must vanish along $z = 1$. The three boundary conditions are then

$$\begin{aligned} &\psi = 0 \quad \text{on} \quad z = 0 \\ &\psi = \frac{d^2\psi}{dz^2} = 0 \quad \text{on} \quad z = 1. \end{aligned} \tag{20}$$

These, taken together with (19), constitute an eigenvalue problem for the complex value of σ as a function of α, V_T and k. The dispersion relation is found by substituting solutions of the form $\exp(irz)$ into (19), finding the three roots of the resulting cubic equation for r exactly and demanding that the conditions (20) be satisfied. This results in a high-order transcendental relation for the complex value of σ, the roots of which are found numerically.

Solutions of (19) with boundary conditions (20) fall into two categories: stationary modes and propagating convection. The former exist for all values of α less than one and for α greater than one when V_T is finite. Propagating modes occur at sufficiently large values of α when V_T is finite. For each horizontal wavenumber k, there are usually many discrete vertical modes. In the case of propagating convection, the largest growth rates are always associated with the gravest vertical mode, while for stationary convection the most unstable mode may have a larger vertical wavenumber, depending on α and V_T. Growth rates and phase speeds of these modes in the case where $k = 5$ are shown in Figs. 3 and 4.

Several features of the eigenvalues are notable. For values of α less than a critical value denoted by the heavy line in Fig. 4 no propagating modes exist and the most unstable stationary mode is the gravest vertical mode. Above this critical value of α, propagating solutions exist and always have the highest growth rates. In this regime, the stationary modes have smaller vertical scales which decrease discretely with increasing α or decreasing V_T. Evidently, the stationary modes are

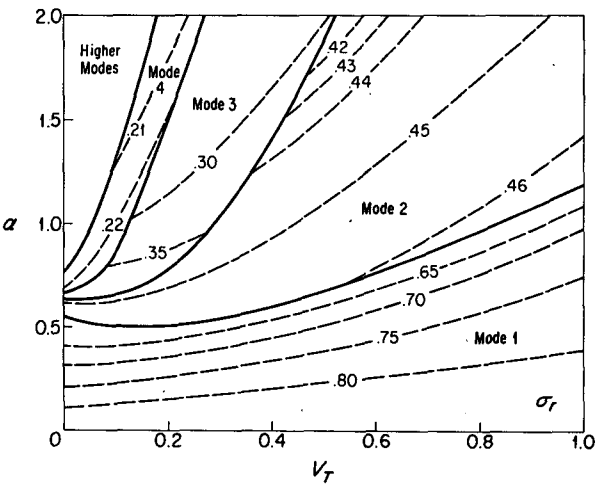

FIG. 3. Dimensionless growth rates of parallel-plate bounded stationary modes as a function of α and V_T for the case $k = 5$. Heavy solid lines denote mode transitions.

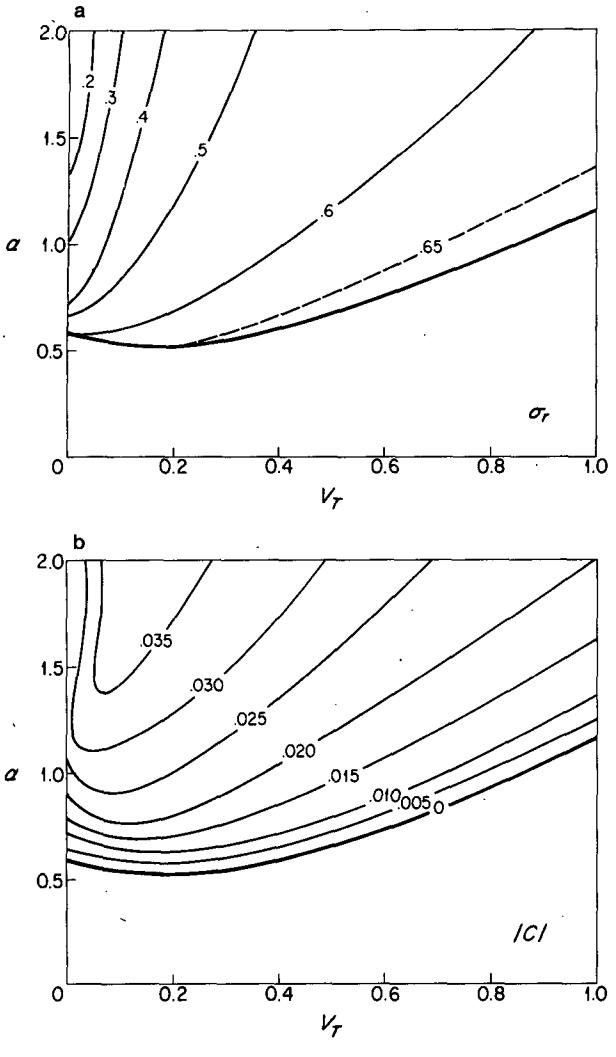

FIG. 4. As in Fig. 3 but (a) for gravest propagating modes. Heavy solid line at bottom shows limit of existence of propagating modes; (b) dimensionless phase speeds.

increasingly dominated by the internal scale $V_T^* N^{-1}$ as V_T becomes small and α increases. Phase speeds of the propagating solutions increase with α except at small values of V_T and $\alpha > 1$ and for a given value of α there always exists some value of V_T which maximizes the phase speed. This is perhaps a result of the particular choice of scaling for the phase speed; Fig. 5 shows the ratio c^*/V_T^* as a function of α and the scaled depth NH/V_T^*. For average atmospheric values of the parameters, phase speeds lie in the range of about 1–5 m s^{-1}.

The transition across $\alpha \approx 0.5$ from stationary, vertical convection to sloped, propagating modes deserves some comment. In the limit of small α, the physics of the instability is similar to that of classical convection. Here the generation of kinetic energy is proportional to the volume average correlation of buoyancy and vertical velocity, $\overline{B'w'}$. The most rapidly growing modes maximize this correlation by maximizing the fraction of kinetic energy that resides in vertical motion; this favors very narrow, upright down- and up-drafts which contain virtually no kinetic energy of horizontal motion. When condensate loading is significant ($\alpha \approx 1$), on the other hand, the generation of kinetic energy is $\overline{B'w'} - g\overline{l'w'}$. There are two competing effects on the optimal slopes of the convective drafts; sloping modes allow condensate to fall out of the updrafts, thus decreasing l' in the updrafts while increasing it in downdrafts, but this occurs at the expense of increasing the amount of kinetic energy in horizontal motion. When α is large enough, the first effect dominates and the most unstable modes are sloped.

Despite the existence of an internal scale $V_T^* N^{-1}$, no short-wave cutoff is found in the inviscid solutions. Figure 6 shows growth rates and phase speeds as functions of wavenumber k for several values of α. Addition of diffusion of heat, water and momentum would provide a short-wave cutoff but would make finding solutions somewhat more difficult. The absence of a short-wave cutoff represents a fundamental limitation of this type of approach, and even the addition of diffusion does not really overcome this limitation, since real convection is fundamentally nonlinear and turbulent. We again stress that while a linear model such as that described here can usefully illuminate the basic physics of a particular process, it cannot by itself provide a comprehensive treatment of the phenomenon. The operation of the basic physical mechanisms suggested by a linear theory should always be subject to verification using observations and more sophisticated nonlinear models.

The structure of the disturbances varies strongly with α and V_T. Some examples of streamlines and precipitation associated with propagating modes are shown in Figs. 7–9, while the structure of the stationary mode is illustrated in Fig. 10. The disturbances always propagate in a direction opposite to the slope of the distur-

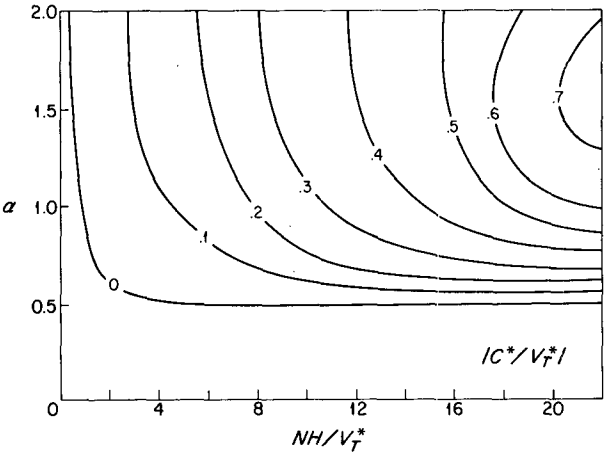

FIG. 5. As in Fig. 4b but showing phase speeds normalized by V_T^* as a function of α and NH/V_T^*.

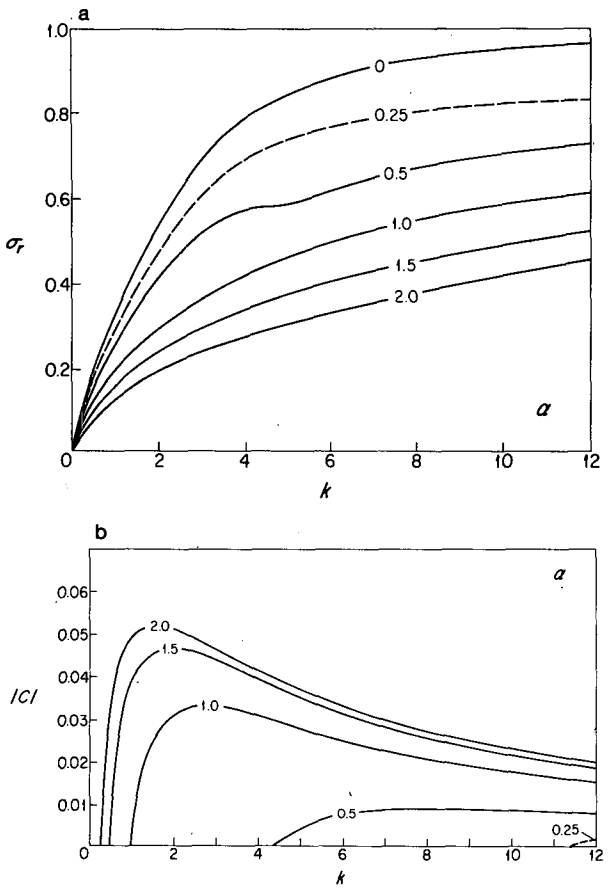

FIG. 6. (a) Dimensionless growth rate as a function of k for $V_T = 0.1$ and several values of α; (b) phase speeds.

bance for the reason elucidated by Seitter and Kuo (1983). Note that Figs. 7 and 8 are for identical values of α, V_T and k. In the first case, the mode appears to be dominated by the internal scale $V_T N^{-1}$ while in the second its depth is more nearly determined by the scale of the domain. When V_T is larger the disturbances tend to have greater velocity amplitude in the upper portion of the cloud, as shown in Fig. 9. In all the propagating modes the rainwater field lags behind and below the updraft. Negative values indicate depletion of the base state cloud water and, as mentioned previously, the linearization forces regions of depleted water as well as surplus water to fall at V_t. This produces an artificial symmetry between upward and downward motion. The stationary mode (Fig. 10) is similar to classical convection except that the velocity amplitude is shifted to higher levels.

The main result of this section is that propagating convection is favored when α is larger than about 0.7, i.e., when the drag exerted by condensate following a reversible displacement is comparable to the thermal buoyancy. Amplifying convection appears to be possible at values of α far exceeding unity; this is because condensate is allowed to fall out of the system. In a strictly calm basic state there is no favored direction of propagation; we show in section 4, however, that vertical shear favors one direction.

While the crudeness of some of the assumptions underlying this analysis make it unwise to apply it to the atmosphere, we can undertake to assess α from vertical soundings. This shows that in the case of middle latitude convection, where thermal buoyancy can be quite large, α is usually much smaller than one and, as Seitter and Kuo (1983) concluded, evaporation of falling rain is far more important. In the tropics, however, the atmosphere is much less unstable and adiabatic water content can be comparable to or even greater than the measured thermal buoyancy. Here the effect of condensate loading and fallout may be more important in determining the form of deep convection.

Perhaps the most unrealistic aspect of the present formulation is the instability for both upward and downward displacements. In nature, much of the rainwater falls in unsaturated air which is stable to (downward) displacements, and without evaporative cooling the water loading would not lead to an unstable downdraft. In our model, the cloud water in the basic state provides enough evaporative cooling to insure instability for both signs of displacement. It is clear that a nonlinear model is necessary to realistically incorporate the effects of evaporating rainwater in unsaturated air. It is, however, possible to examine some effects of evaporation by incorporating into the basic state a subsaturated layer below cloud base. This is discussed presently.

3. Effects of subcloud evaporation

To include the effects of evaporation below cloud base we redefine the basic state as in Fig. 11. The upper layer consists of an unstable uniform cloud, as in the preceding analysis. The lower layer is subsaturated and neutrally stratified. Rain falling into this layer from above is allowed to evaporate at a rate proportional to the amount present.

The linearized equations for the cloud layer are identical to those presented in section 2 and we normalize the variables in both layers according to (18). The nondimensional equations for vorticity, thermal buoyancy and liquid water in the lower layer are

$$\sigma\left(\frac{d^2\psi}{dz^2} - k^2\psi\right) = ik(B - \alpha l), \tag{21}$$

$$\sigma B = -\alpha EMl, \tag{22}$$

$$\left(\sigma - V_T\frac{d}{dz}\right)l = -El, \tag{23}$$

where E is the evaporation rate normalized by N (of the cloud layer) and M is proportional to the heat of vaporization:

$$M \equiv L_v/C_pT_0,$$

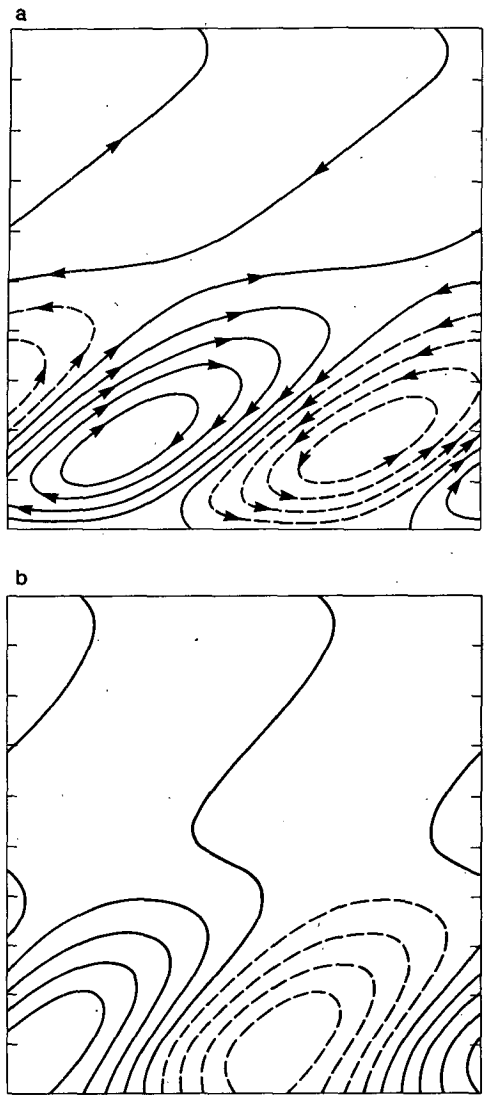

FIG. 7. (a) Streamfunction (normalized to have an amplitude of 1.0) associated with mode dominated by internal vertical scale V_T^*/N, for $\alpha = 2.0$; $V_T = 0.032$ and $k = 2.1$; modes shown move from right to left at a dimensionless speed of 0.026; growth rate is 0.112. (b) Liquid water perturbation associated with mode shown in (a); dimensionless amplitude is 8.0 times the streamfunction amplitude.

where L_v is the latent heat of vaporization, C_p the heat capacity at constant pressure and T_0 is a reference subcloud layer temperature.

Solutions to the system comprised of (19) in the cloud layer and (21)–(23) in the subcloud layer together with the boundary conditions (20) can be found by matching vertical displacement, pressure and liquid water content across cloud base. Once again it is possible to find an exact dispersion relation, but solutions of the highly transcendental equation must be found numerically.

The complete system is described by the dimensionless parameters α, V_T, E and Z_b, where the last is the dimensionless height of the cloud base. As this is too large a parameter space to explore at all thoroughly, we instead present specific examples of solutions.

We find that the most rapidly growing solutions fall into two categories which we shall designate as the "cloud mode" and the "subcloud mode," respectively. The first is simply a modification of the type of solution discussed in the previous section while the second is a new feature.

An example of the streamlines associated with the cloud mode is presented in Fig. 12. Here the subcloud layer extends through only a tenth of the depth of the domain, but evaporation is just strong enough to produce a secondary maximum in the streamfunction within the subcloud layer. For modes with small growth

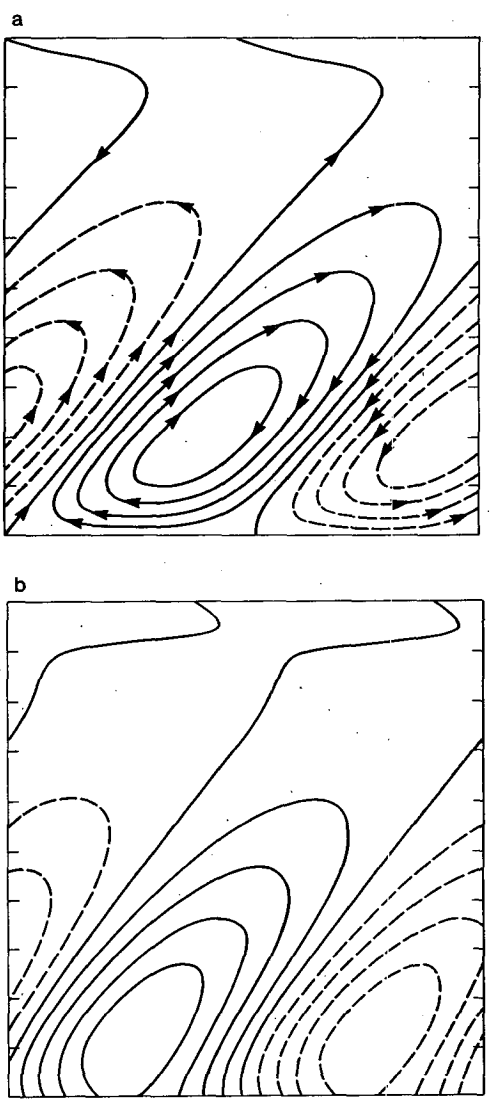

FIG. 8. As in Fig. 7a but for mode dominated by external vertical scale H; mode moves from right to left at dimensionless speed of 0.042 and has growth rate of 0.108. (b) Perturbation liquid water for mode shown in (a); dimensionless amplitude is 8.0.

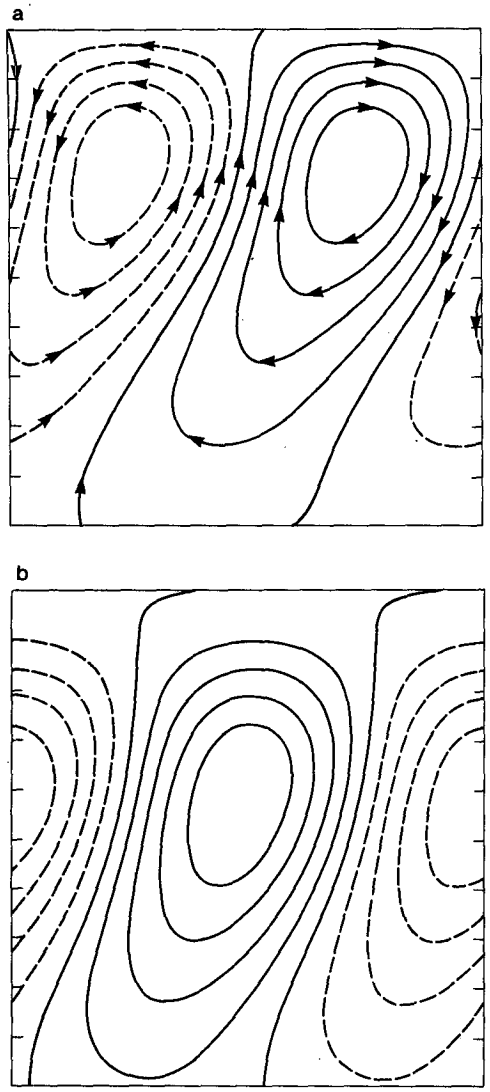

FIG. 9. (a) Example of streamfunction (with normalized amplitude of 1.0) when $\alpha = 0.5$, $V_T = 0.1$ and $k = 6.0$; mode shown moves from right to left at a speed of 0.008 and has a growth rate of 0.625. (b) Liquid water perturbation associated with mode shown in (a); amplitude = 7.72.

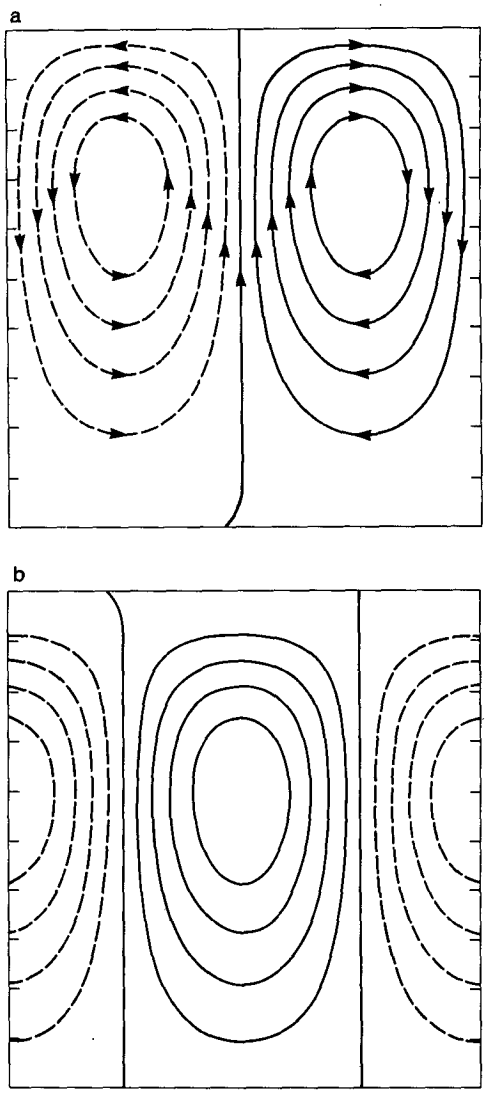

FIG. 10. (a) Example of streamfunction of stationary mode for $\alpha = 0.5$, $V_T = 0.05$ and $k = 6.0$; growth rate is 0.618. (b) Liquid water perturbation associated with mode shown in (a); amplitude = 9.0.

rates this feature represents a linear analog to a gust front with the main momentum balance being between the horizontal pressure gradient force and the inertial acceleration:

$$c\frac{\partial u'}{\partial x} \approx \frac{1}{\rho_0}\frac{\partial p'}{\partial x},$$

where c is the phase speed and u' and p' are perturbation horizontal velocity and pressure, respectively. In this example, the presence of the "gust front" does not appreciably change the growth rate or phase speed of the solution and in this respect it represents a minor modification of the modes discussed in Section 2.

The perturbation pressure field associated with the streamlines of Fig. 12 is presented in Fig. 13. The major pressure perturbation seems to be associated with the subcloud layer cooling while above cloud base the pressure has roughly the distribution that would be calculated hydrostatically from the buoyancy field. The pressure perturbations shown in Fig. 13 bear a remarkable resemblance to those deduced within a trop-

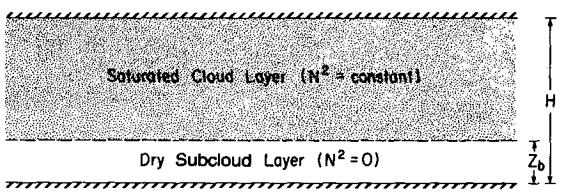

FIG. 11. Basic state containing uniform cloud in upper region of constant static instability and a neutrally stratified unsaturated subcloud layer.

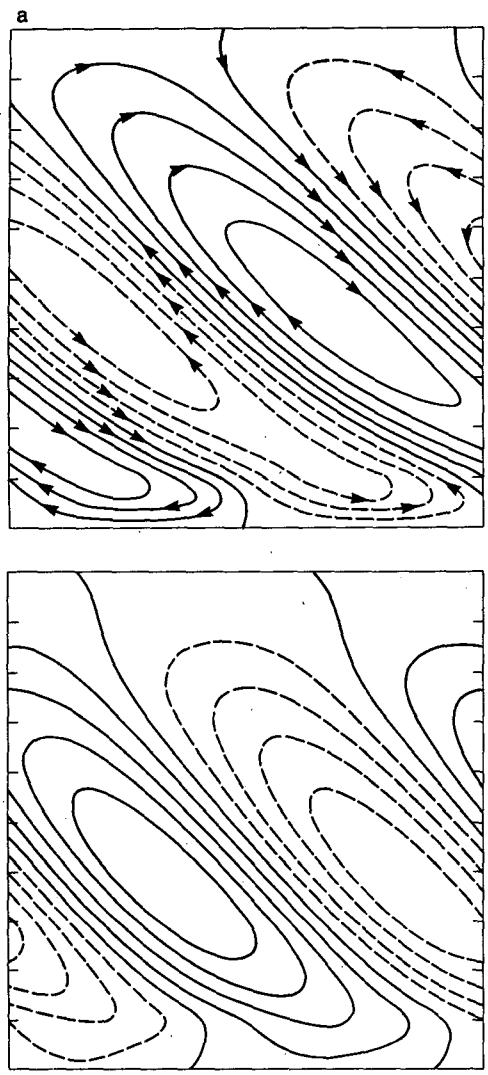

FIG. 12. (a) Streamfunction (normalized to have an amplitude of 1.0) associated with "cloud mode" for $\alpha = 1.0$, $V_T = 0.1$, $E = 0.5$ and $k = 8.0$; mode moves from left to right with a dimensionless speed of 0.022 and growth rate of 0.535; depth of subcloud layer is 0.1. (b) Perturbation liquid water associated with mode shown in (a); amplitude = 8.45.

ical squall line by LeMone et al. (1984b); see Fig. 14. Here the low-level perturbations are no doubt associated with subcloud cooling, and we wish to suggest that the slope and magnitude of the pressure distribution aloft is also related to phase-lagged buoyancy effects associated with falling precipitation, though in nature these may be associated more with evaporative cooling than with condensate loading. It is perhaps worth noting that the phase speed and slope of the tropical squall line are in quantitative agreement with the linear model. (Assuming that $H \approx 10$ km and $N \approx 10^{-2}$ s^{-1}, the mode in Figs. 12 and 13 moves at about 2.2 m s^{-1}, which can be compared to the composite speed of 2.2 m s^{-1} reported by Barnes and Sieckman, 1984.)

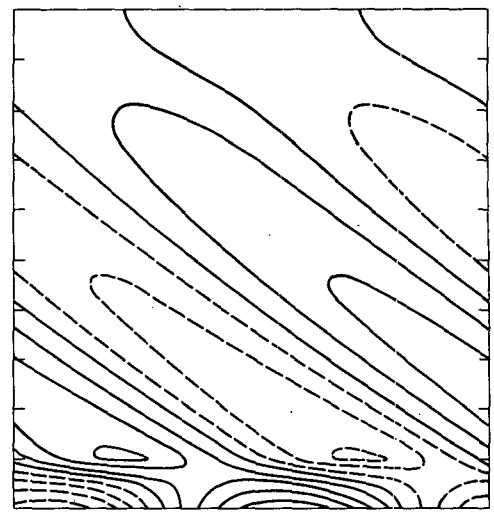

FIG. 13. Pressure perturbation associated with mode shown in Fig. 12; amplitude = 1.14 times the streamfunction amplitude.

It is apparent that whatever asymmetries in nature might determine the direction of propagation of the modes discussed here and in section 2 also determine the sign of the vertical transport of horizontal momentum. As the slopes of the streamlines shown here are order one it is clear that the vertical flux of horizontal momentum is quite large and, in the case of convection in a calm environment, completely uncorrelated with environmental winds. We wish to suggest that the large momentum fluxes reported by LeMone (1983) and others are consequences of phase-lagged buoyancy effects due to falling precipitation. More will be said about this in section 4.

An example of the subcloud layer mode which appears in the model is shown in Fig. 15. This mode is

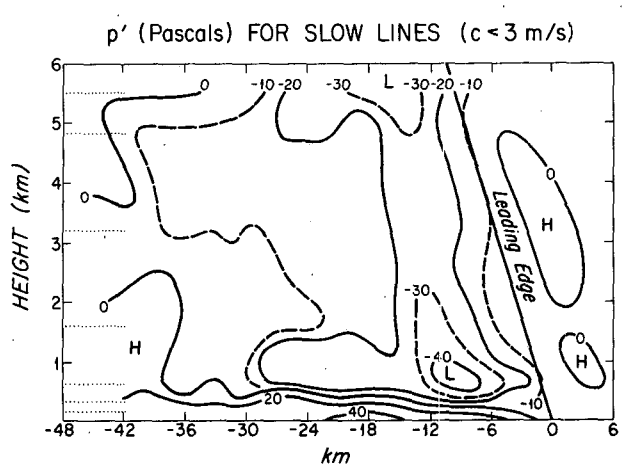

FIG. 14. Composite pressure perturbation (P'_a) relative to inflow environment for slow-moving tropical squall lines. Sloping line indicates position of leading edge of clouds associated with squall. Dotted lines at left indicate average flight levels of aircraft. Note vertical scale exaggeration of 6:1. [From LeMone et al. (1984b)].

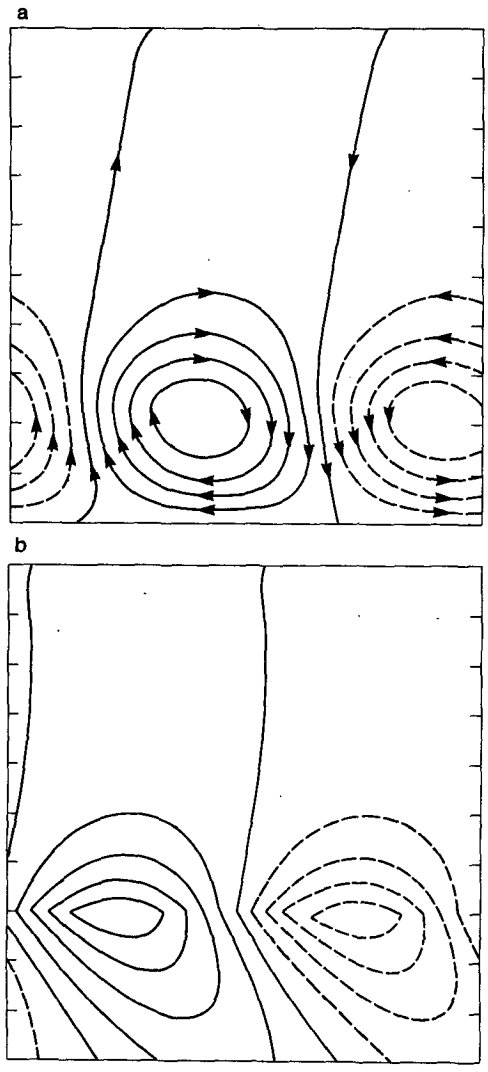

FIG. 15. (a) Streamfunction associated with "subcloud mode" for $\alpha = 1.0$, $V_T = 0.1$, $E = 0.25$ and $k = 4.0$; depth of subcloud layer is 0.3; mode shown travels from right to left with a dimensionless speed of 0.111 and has a growth rate of 0.173. (b) Liquid water perturbation associated with mode shown in (a); amplitude = 2.73.

almost entirely confined to the subcloud layer and it propagates at much larger velocities and has smaller growth rates than do the cloud modes. Just enough condensation occurs within the cloud layer to produce falling precipitation whose evaporation drives this mode. Even so, it is somewhat surprising that the amplitude is so small within the cloud layer in view of its instability and the neutral stratification of the subcloud layer. This mode is almost certainly an artifact of the model, since in nature a much deeper perturbation within the cloud layer would be necessary to cause precipitation. The shallowness of the perturbation within the cloud is related to the large propagation speed of the "gust front"; this aspect of the coupling between cloud and subcloud layers is the subject of the next section.

4. Precipitating convection with mean wind shear

It is well known from previous studies of linear nonprecipitating convection (e.g., Kuo, 1963) that the addition of a constant mean vertical shear of the horizontal wind to the Rayleigh basic state leads to a diminution of the growth rates of the convective disturbances, which tend to line up with the shear. The only instances in which cross-shear modes dominate are those in which the shear profile has an inflection point at which the shear is a maximum; in these cases the cross-shear modes are driven primarily by the shear itself and are clearly separable from the along-shear convective modes (Asai, 1972). Hathaway and Somerville (1985) have also recently demonstrated that a strong horizontal component of the Coriolis parameter at right angles to the mean shear vector may lead to dominant cross-shear modes, though it is unlikely that this effect is significant in the earth's atmosphere.

The decoupling of buoyancy production from vertical velocity in precipitating convection was shown by Seitter and Kuo (1983) to allow the convection to extract kinetic energy from the mean shear and this implies that the most unstable modes of precipitating convection may be aligned across the shear. In principle, this point could be made in the context of the present linear formulation by adding a constant mean shear to the basic states described in the preceding section. The nonhomogeneity of the resulting linear equations introduces complications, however, which make solution more difficult than is probably justified in so crude a model. We therefore choose instead to represent mean shear by a discontinuous jump in mean velocity at cloud base, z_b. This presents its own problems, since a discontinuous velocity profile is subject to many shearing instabilities even when the stratification is stable. We shall avoid this problem, however, by considering only those unstable modes which have no critical layer where their phase speed matches the velocity of the mean flow. That is, we shall examine relatively deep disturbances whose phase speeds fall outside the range of velocities of the mean flow; these disturbances do not satisfy the semicircle theorem of Howard (1961) and are thus specifically related to the presence of precipitation.

The modification to the basic state discussed in section 3 consists simply in adding a right-to-left mean velocity U to the cloud layer in Fig. 11. The resulting dimensionless equations are identical to the set including (19) and (21)–(23) with boundary conditions (20) except that the growth rate σ appearing in (19) is replaced by the Doppler shifted complex expression $\sigma + ikU$. The vertical displacement, pressure and liquid water are all matched across the interface at z_b. Note that in general the streamfunction itself will be discontinuous across z_b.

The variations of the growth rates and phase speeds of both the subcloud and cloud modes with increasing

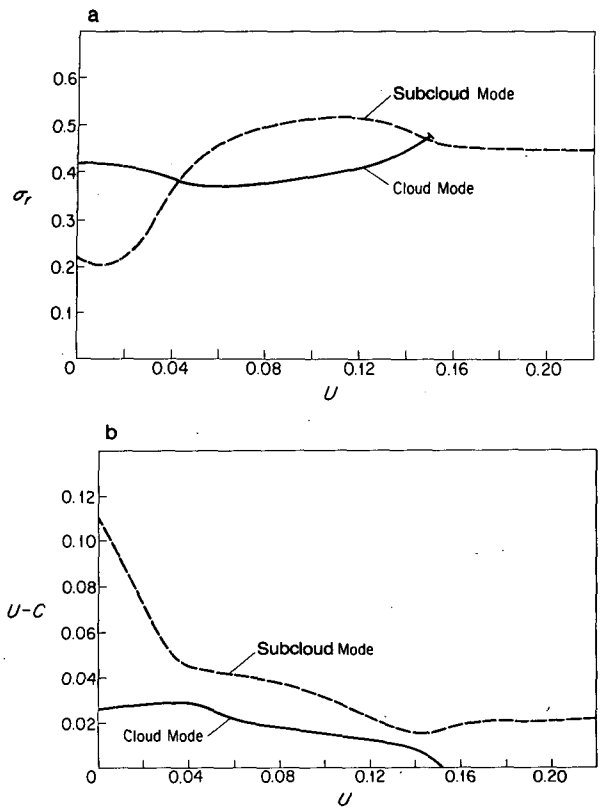

FIG. 16. Variation of growth rate (a) and absolute value of difference between cloud layer wind U and phase speed c (b) with U for $\alpha = 1.0$, $V_T = 0.1$, $E = 0.5$, $z_b = 0.2$ and $k = 5.0$.

shear are shown in Fig. 16 for particular values of E, V_T, α and z_b. As the shear increases, the growth rate of the cloud mode remains relatively constant while that of the subcloud mode increases. At some particular value of the shear, the growth rates of the two modes are equal; above this value the subcloud mode has higher growth rates. Above a critical shear value, the growth rate of the subcloud mode begins to decrease again. As shown in Fig. 16b, the phase speed of the cloud mode becomes smaller than the mean velocity U of the upper layer when U is sufficiently large; at this point the cloud modes have critical layers and interpretation of the solutions becomes somewhat more difficult.

The streamlines associated with the subcloud mode are shown in Fig. 17. As the shear increases, the subcloud mode extends further into the cloud layer, indicating a closer coupling of the evaporatively driven downdraft and the cloud layer instability. The problem of precipitation from a very shallow layer is alleviated. The phase shift across the shear level is upshear, indicating a downgradient momentum transport. Since such a downgradient transport is forbidden for nonprecipitating modes without critical levels (Kuo, 1963), the present results constitute a linear proof of the Seitter–Kuo hypothesis.

The growth rates and phase speeds of the most unstable mode are shown in Fig. 18 as a function of the nondimensional evaporation rate E and the mean vertical shear between the cloud and subcloud layers. The highest growth rates occur for particular combinations of the evaporation rate and the shear. The heavy dashed line at the left of Fig. 18 separates the cloud and subcloud modes.

Note that the transition from cloud to subcloud mode at the left of Fig. 18 also denotes a weak minimum of growth rate. This implies that for relatively weak shear the preferred mode of convection in this model is shear-parallel lines. This is because while weak shear normal to the lines reduces the growth rate of the convection, a component of shear parallel to the lines has no effect whatever on the growth rates (e.g., see Kuo, 1963). Thus for a given weak shear, there will be a weak tendency in the linear model for convection to avoid having a perpendicular component of shear. For stronger shears (to the right of the dotted line in Fig. 18) the growth rates exceed those of the no-shear (or shear-parallel) modes and thus the linear model exhibits a preference for modes which line up perpendicular to the shear.

To the right of the growth rate maximum in Fig. 18 the growth rates decline with increasing shear. In this regime, the most unstable modes will be rotated in the x–y plane such that the *perpendicular* component of shear remains at the optimum value shown in Fig. 18. The symmetry of the mean flow is such that the direction of rotation of the modes away from the y axis is immaterial; both clockwise and counterclockwise rotations that reduce the orthogonal component of shear to its optimum value will result in modes with maximum growth rates. This implies that convection in this regime will in general be three dimensional.

The aforementioned results together with a few additional calculations allow the construction of a tentative model regime diagram, shown in Fig. 19. This diagram has either evaporation rate or subcloud layer depth along the ordinate and low-level shear along the abscissa and pertains to moderate values of α, V_T and horizontal wavenumber. For sufficiently small shear, two-dimensional convection with roll axes aligned with the shear is preferred. At intermediate values of the shear convection takes the form of two-dimensional lines with roll axes aligned across the direction of the vertical shear. At very large shears three-dimensional convection is preferred.

5. Comparison with observations and conclusions

The obvious limitations of linear theory prevent a detailed comparison of the present results with nature. As stated in the Introduction, our purpose has been to illustrate some of the key dynamical processes which serve to distinguish precipitating moist convection from the nonprecipitating variety, without claiming to have

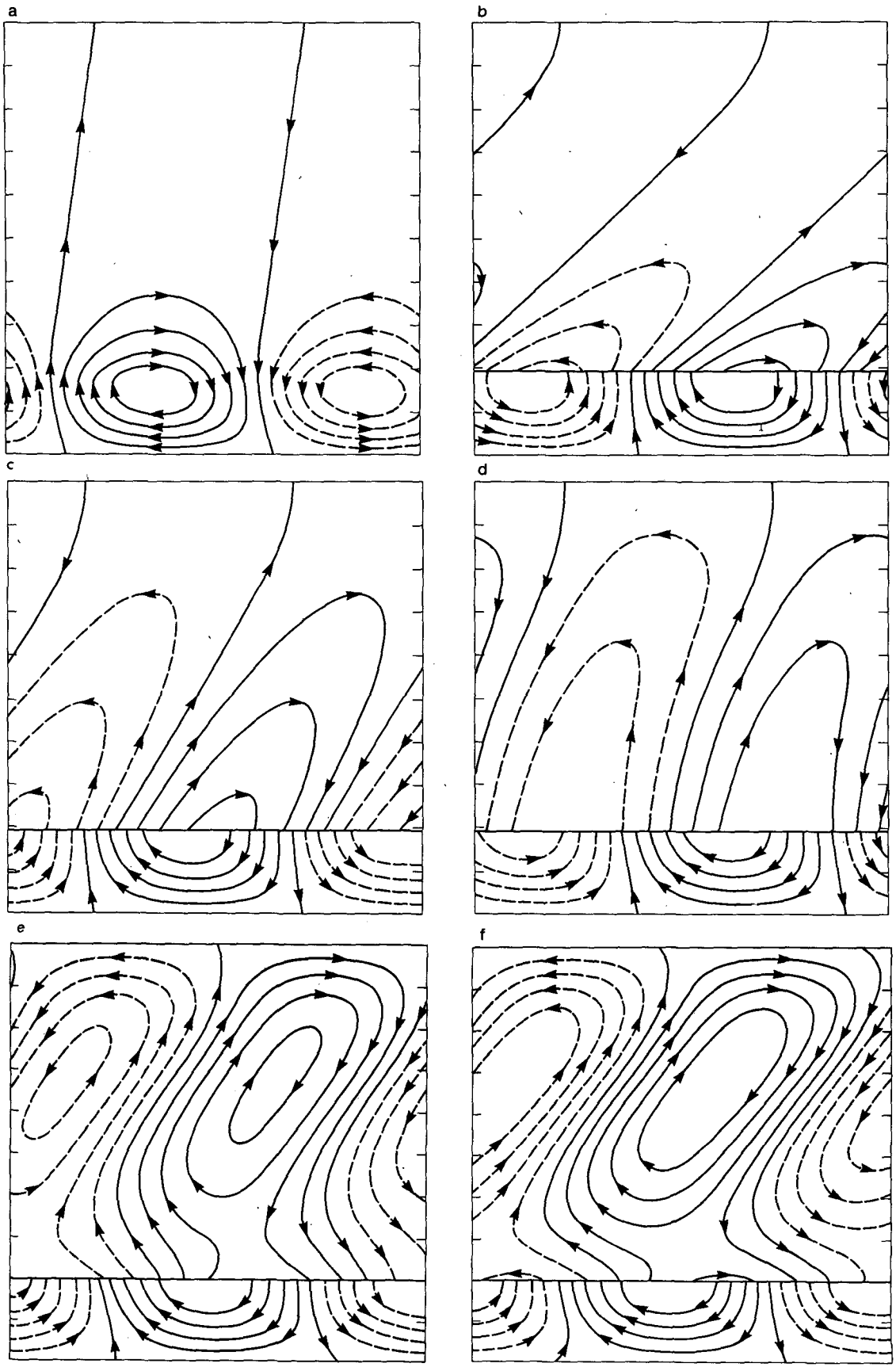

FIG. 17. Variation of streamfunction with cloud-layer/subcloud-layer shear for $\alpha = 1.0$, $V_T = 0.1$, $E = 0.5$, $z_b = 0.2$ and $k = 5.0$. Cloud-layer wind and phase speed of modes is from right to left. (a) $U = 0.0$, (b) $U = -0.04$, (c) $U = -0.08$, (d) $U = -0.12$, (e) $U = -0.16$, (f) $U = -0.20$.

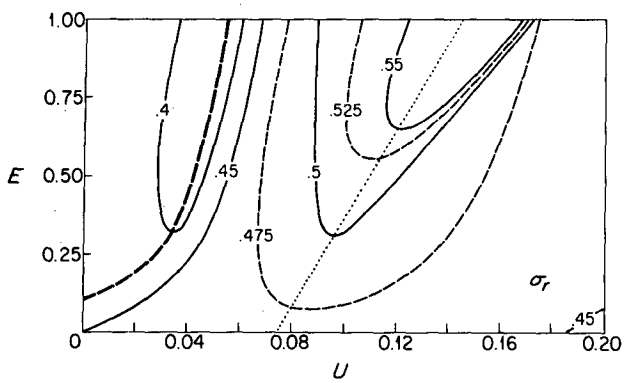

FIG. 18. Dimensionless growth rate as a function of evaporation rate E and cloud-layer/subcloud-layer shear U for $\alpha = 1.0$, $V_T = 0.1$, $z_b = 0.2$ and $k = 5.0$. Growth rates to left of heavy dashed line at left are associated with the "cloud mode"; all others pertain to "subcloud" mode. Dotted line denotes growth rate maximum.

in any way simulated the complex processes at work within clouds. As such, our conclusions are at best suggestive. We, nevertheless, maintain that certain *qualitative* aspects of convection within our simple model have counterparts in nature to the extent that the physics of the model captures the essence of the dynamics of actual precipitating convective systems. What we believe are the important qualitative, testable hypotheses that follow from the present work are enumerated as follows:

1) Weakly buoyant precipitating convective lines may exhibit substantial slopes with respect to the vertical, even in the absence of mean shear, and should propagate slowly with respect to the mean cross-line flow in a direction determined by the slope, with the bottom part of the convective line advancing first.

2) In environments characterized by weak shear in the lower troposphere, weakly buoyant convective lines should exhibit a tendency to align with the mean shear. Their propagation across the direction of the shear will be relatively slow (i.e., a few m s^{-1}).

3) In environments with moderate vertical shear in the lower troposphere, precipitating convection can extract kinetic energy from the mean flow (as shown originally by Seitter and Kuo, 1983) and should thus exhibit a preference to occur in the form of lines oriented across the vertical shear in the lower troposphere.

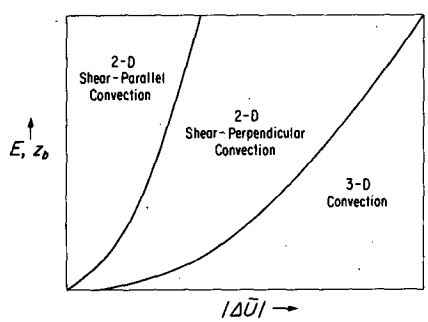

FIG. 19. Qualitative model regime diagram. Evaporation rate and/or subcloud-layer depth shown on ordinate while cloud-layer/subcloud-layer shear appears on abscissa.

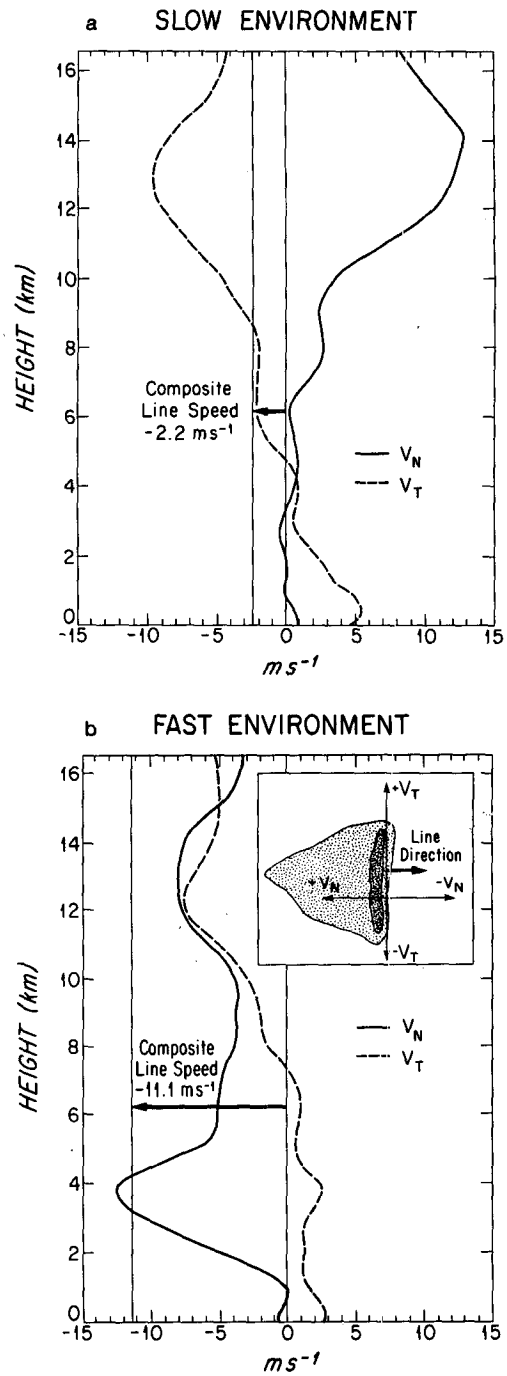

FIG. 20. Composite profiles of ground-relative wind component normal (V_N, solid) and parallel (V_T, dashed) to leading edge of slow (a) and fast (b) tropical squall lines. Thin vertical line shows mean ground-relative propagation speeds of the lines. Definition of coordinate system shown in inset of (b). [From Barnes and Sieckman (1984)].

The mean shear allows the cloud-layer convection to couple closely with the evaporatively driven gust front near the surface. In this regime, convective lines propagate downshear and the present work predicts propagation speeds slightly greater than the mean wind in the cloud layer. Such convective lines transport horizontal momentum *down* the low-level gradient.

4) When the shear in the lower troposphere is quite large, convective lines, if they occur, should exhibit a preference for an orientation which is skewed with respect to the low-level shear; otherwise, three-dimensional convection is indicated.

In the context of the present work, these results apply to weakly buoyant convection [$\alpha \approx O(1)$]; upright, three-dimensional convection is indicated for strongly buoyant ($\alpha \ll 1$) conditions. By "weak," "moderate," and "strong" shear we are in this instance comparing the low-level vertical shear with a measure of the evaporation rate of rain falling into subcloud air. Specifically, as indicated by Fig. 18, the regime of convection depends mostly on the parameter U/E which is dimensionally equivalent to $\Delta U^*/E^*h$, where E^* is a measure of the evaporation rate, h^* is the depth of the subcloud layer, and ΔU^* is the total change of mean wind across the lower troposphere.

Points 1 through 3 are consistent with observations of tropical squall lines reported recently by LeMone et al. (1984b), Barnes and Sieckman (1984) and LeMone et al. (1984a). They divided the observed squall lines into two categories: slow-moving lines, which tend to align with the mean shear and move across it at speeds generally less than 3 m s^{-1} (with respect to the ground); and fast-moving lines which form in environments which exhibit strong low-level jets. The fast-moving lines are aligned across the direction of the low-level jet and tend to move at speeds close to the maximum jet speed, as noted also by Bolton (1984) and Fernandez (1980). Composite environmental wind structures for both lines are reproduced in Fig. 20. LeMone et al. (1984a) note that both types of squall line exhibit pronounced slopes in the vertical plane; the direction of slope is opposite the propagation direction as in the results of the present model. These slopes are associated with vertical transports of cross-line horizontal momentum which may be uncorrelated with the mean vertical shear, especially in the case of the slow-moving lines (LeMone et al., 1984b).

The main difference between the environments of fast- and slow-moving lines seems to lie in their respective kinematic structures. Barnes and Sieckman (1984) show that the total change in environmental wind speed in the lowest 4 km is about twice as large in the case of fast lines as it is when slow lines are observed; as noted before, the fast lines are oriented normal to the low-level shear while the slow lines tend to be aligned with the shear. Differences in the thermodynamic environments of the two classes of lines appear to be somewhat more subtle, with the slow lines appearing to form in environments with marginally greater convective available potential energy (CAPE) than the environments of fast lines exhibit.

LeMone et al. (1984b) have calculated vertical fluxes of horizontal momentum using aircraft data. Data from a fast line case (GATE Day 255) clearly show that the cross-line momentum fluxes are downgradient in the lowest 3 km but upgradient in the middle and upper troposphere. The vertical flux of line-parallel momentum is, on the other hand, always downgradient.

The slope, propagation, and environmental characteristics of observed tropical squall lines are clearly consistent with the qualitative, testable predictions of the present linear model. Comparison of predicted and observed perturbation pressure fields (Figs. 13 and 14) lends further credence to the basic thesis on which the model is founded; namely, that the slope and propagation of certain precipitating convective lines are due to the decoupling of buoyancy sinks from the vertical velocity field. Comprehensive tests of these ideas must, however, await further detailed simulation of tropical squall lines using sophisticated numerical models.

Acknowledgments. In preparing this work, the author profited from numerous discussions with Drs. Edward Zipser, Peggy LeMone, Gary Barnes, Rich Rotunno, Dave Raymond, Mitch Moncrieff, Martin Miller, Alan Thorpe and Chris Bretherton. This work was supported by NSF Grants ATM-8313454 and ATM-8513171.

REFERENCES

Asai, T., 1970a: Three-dimensional features of thermal convection in a plane Couette flow. *J. Meteor. Soc. Japan,* **48,** 18–29.

——, 1970b: Stability of a plane parallel flow with variable vertical shear and unstable stratification. *J. Meteor. Soc. Japan,* **48,** 129–139.

——, 1972: Thermal instability of a shear flow turning the direction with height. *J. Meteor. Soc. Japan,* **50,** 525–532.

Barnes, G. M., and K. Sieckman, 1984: The environment of fast- and slow-moving tropical mesoscale convective cloud lines. *Mon. Wea. Rev.,* **112,** 1782–1794.

Bluestein, H. B., and M. H. Jain, 1985: Formation of mesoscale lines of precipitation: Severe squall lines in Oklahoma during the spring. *J. Atmos. Sci.,* **42,** 1711–1732.

Bolton, D., 1980: Application of the Miles Theorem to forced linear perturbations. *J. Atmos. Sci.,* **37,** 1639–1642.

——, 1984: Generation and propagation of African squall lines. *Quart. J. Roy. Meteor. Soc.,* **110,** 695–721.

Bretherton, C. S., 1986: A theory for nonprecipitating moist convection between parallel plates. *J. Atmos. Sci.* (to be published)

Browning, V. A., and F. H. Ludlam, 1962: Air flow in convective storms. *Quart. J. Roy. Meteor.,* **88,** 117–135.

Deardorff, J. W., 1965: Gravitational instability between horizontal plates with shear. *Phys. Fluids,* **8,** 1027–1030.

Durran, D. R., and J. B. Klemp, 1982: On the effects of moisture on the Brunt-Väisälä frequency. *J. Atmos. Sci.,* **39,** 2152–2158.

Emanuel, K. A., 1982: Inertial instability and mesoscale convective systems. Part II: Symmetric CISK in a baroclinic flow. *J. Atmos. Sci.,* **39,** 1080–1097.

——, 1984: Some dynamical aspects of precipitating convection. *Dynamics of Mesoscale Weather Systems,* NCAR, 591 pp.

Fernandez, W., 1980: Environmental conditions and structure of some types of convective mesosystems observed over Venezuela. *Arch. Meteor. Geophys. Bioklim.* **A29,** 249–267.

Hathaway, D. H., and R. J. C. Somerville, 1985: Nonlinear interaction between convection, rotation and flows with vertical shear. *J. Fluid Mech.,* (in press).

Howard, L. N., 1961: Note on a paper of John W. Miles. *J. Fluid Mech.,* **10,** 509–512.

Kessler, E., 1969: *On the Distribution and Continuity of Water Substance in Atmospheric Circulation. Meteor. Monogr.,* No. 32, Amer. Meteor. Soc., 84 pp.

Kuo, H.-L., 1963: Perturbations of plane Couette flow in stratified fluid and origin of cloud streets. *Phys. Fluids,* **6,** 195–211.

——, and K. L. Seitter, 1985: Instability of shearing geostrophic currents in neutral and partly unstable atmospheres. *J. Atmos. Sci.,* **42,** 331–345.

LeMone, M. A., 1983: Momentum transport by a line of cumulonimbus. *J. Atmos. Sci.,* **40,** 1815–1834.

——, G. M. Barnes, E. J. Szoke and E. J. Zipser, 1984a: The tilt of the leading edge of mesoscale tropical convective lines. *Mon. Wea. Rev.,* **112,** 510–519.

——, —— and E. J. Zipser, 1984b: Momentum flux by lines of cumulonimbus over the tropical oceans. *J. Atmos. Sci.,* **41,** 1914–1932.

Lilly, D. K., 1960: On the theory of disturbances in a conditionally unstable atmosphere. *Mon. Wea. Rev.,* **88,** 1–17.

Lindzen, R. S., 1974: Wave–CISK in the tropics. *J. Atmos. Sci.,* **31,** 156–179.

Moncrieff, M. W., 1981: A theory of organized steady convection and its transport properties. *Quart. J. Roy. Meteor. Soc.,* **107,** 29–50.

——, and M. J. Miller, 1976: The dynamics and simulation of tropical cumulonimbus and squall lines. *Quart. J. Roy. Meteor. Soc.,* **102,** 373–394.

Nehrkorn, T., 1986: Wave–CISK in a baroclinic basic state. *J. Atmos. Sci.,* **43,** (in press).

Newton, C. W., 1950: Structure and mechanism of the pre-frontal squall line. *J. Meteor.,* **7,** 210–222.

Raymond, D. J., 1975: A model for predicting the movement of continuously propagating convective storms. *J. Atmos. Sci.,* **32,** 1308–1317.

——, 1976: Wave–CISK and convective mesosystems. *J. Atmos. Sci.,* **33,** 2392–2398.

——, 1983: Wave–CISK in mass flux form. *J. Atmos. Sci.,* **40,** 2561–2572.

——, 1984: A wave–CISK model of squall lines. *J. Atmos. Sci.,* **41,** 1946–1958.

Rotunno, R., and J. B. Klemp, 1982: The influence of shear-induced pressure gradient on thunderstorm motion. *Mon. Wea. Rev.,* **110,** 136–151.

Seitter, K. L., and H.-L. Kuo, 1983: The dynamical structure of squall-line type thunderstorms. *J. Atmos. Sci.,* **40,** 2932–2854.

Zipser, E. J., 1977: Mesoscale and convective-scale downdrafts as distinct components of squall-line circulation. *Mon. Wea. Rev.,* **106,** 789–805.